euspen's 25th International Conference & Exhibition, Zaragoza, ES, June 2025
www.euspen.eu

Two shear-shift absolute test of reference error for white-light interferometers

ZUBO HU[1, 2, 3], SHUAI XUE[1, 2, 3*], YUNFENG MAO[1, 2, 3], YIHANG HUANG[1, 2, 3], JIAJUN CAI[1, 2, 3], AND YIFAN DAI[1, 2, 3]

[1] *College of Intelligence Science and Technology, National University of Defense Technology, Changsha, Hunan, 410073, China*
[2] *Hunan Key Laboratory of Ultra-Precision Machining Technology, Changsha, Hunan, 410073, China*
[3] *National Key Laboratory of Equipment State Sensing and Smart Support, National University of Defense Technology, Changsha, Hunan, 410073, China*

**shuaixue1990@163.com*

Abstract
Next generation of advanced sources including diffraction-limiting synchrotron radiation and free electron laser posed slope accuracy better than 50 nrad and 2 nm Peak-to-Valley (PV) height form accuracy. The spatial resolution for controlling the slope error is approaching sub-millimeter, thus the precise measurement of the mid-frequency holds significant. Due to the relatively lower instrument transfer function (ITF) of wavefront interferometers when testing the mid-frequency error, wavefront interferometers can hardly meet the strict slope and PV height accuracy. White-light interferometers (WLIs) gain advantages of higher resolution, higher ITF and higher repeatability. Therefore, Micro Stitching Interferometry (MSI) utilizing WLIs have been widely used to test X-ray surfaces. As the test results is relative to the reference surface, it is essential to calibrate the reference error of the WLIs. For this end, random flats method is commonly utilized, however, this method requires the translation distances of the test surface greater than the correlation length of the tested surface. However, the correlation length of the test surface is usually unknown, and the inappropriate test parameters will introduce unneglected errors. To address this, a two shear-shifts absolute test method for WLIs is applied. This method is conducted by performing at least two measurements with the test surface translated along the two orthogonal directions with different distances of integer pixels, respectively. Together with the measurement performed at the initial position, five measurements in total are required. The absolute test algorithm model has been established, and the simulation verifications have been conducted. The reference surface of a Zygo NewView 9000 1× objective lens with 8.6 mm aperture was calibrated using the proposed method. The measurement repeatability and robustness of this method was verified using test flats with different topology precisions and different processing techniques. The accuracy of the method was verified by comparing the calibration results with that obtained by random flats method utilizing a flat with extreme form accuracy. The results indicate that the method can achieve sub-nanometer and nanoradian accuracy, which meets the reference surface calibration accuracy requirements posed by the surfaces of the next generation light sources.

X-ray mirrors, white light interferometer, absolute test, two shear-shifts

1. Introduction

Advanced light sources constitute indispensable tools for fundamental scientific investigations. Next generation diffraction-limited synchrotron radiation sources and free-electron lasers impose stringent specifications on X-ray mirror fabrication, necessitating surface figure accuracy exceeding 2 nm peak-to-valley (PV) height and 50 nrad root-mean-square (RMS) slope precision. To address these requirements, precision surface finishing techniques including ion beam figuring (IBF) and elastic emission machining (EEM) have been developed [1, 2]. The characterization of mid-spatial frequency errors during surface metrology represents a critical challenge in this context. The instrument transfer function (ITF) serves as a quantitative metric for evaluating measurement systems' capacity to resolve such errors [3]. White-light interferometers (WLIs), characterized by superior lateral resolution, enhanced ITF performance, and measurement repeatability, have become prevalent for strongly curved surface inspection [4]. However, their implementation requires preliminary absolute calibration of reference surfaces. Conventional random flats calibration methodologies demand reference flats with exceptional surface quality—a requirement frequently unattainable for most research facilities [5-7]. Furthermore, this approach theoretically requires translation distances exceeding the test flat's correlation length [8], a parameter generally unspecified in practice, potentially introducing substantial measurement uncertainties. This limitation underscores the necessity for developing absolute calibration methods capable of determining WLI reference errors without relying on surfaces superior to the test specimens. The shear-shift methodology, successfully implemented in phase-shifting interferometry, demonstrates potential applicability for WLI calibration [9-14]. This technique eliminates both the requirement for calibration flats surpassing test surface accuracy and prior knowledge of the calibration flat's surface characteristics. Nevertheless, its adaptation to WLI reference calibration remains undocumented in existing literature. For effective deployment of WLIs in X-ray mirror metrology, achieving calibration accuracies of approximately 1 nm PV and 0.2 nm RMS becomes imperative. This study introduces a two-dimensional shear-shift (TSS) absolute calibration method specifically designed for WLI reference surfaces. We establish the mathematical framework governing this technique and identify optimal operational parameters through systematic analysis. Experimental validation confirms the TSS method's effectiveness in reference surface calibration, thereby providing a robust methodology for ensuring WLI measurement traceability and advancing X-ray mirror fabrication technologies.

2. Mathematical model of TSS

Single shear-shift absolute method seems to be the simplest shear-shift absolute test method [12]. As shown in Figure 1(a), the reference surface keeps stationary, and the test flat is tested at three positions, i.e., the basic position (P_0), two positions with translation of integer pixels along x and y (P_x and P_y). The test results are denoted as $\mathbf{M}_0$, $\mathbf{M}_x$, $\mathbf{M}_y$, respectively. The translation distances of P_x, P_y relative to P_0 are d_x, d_y, respectively. Note $d_x = n_x \cdot \varepsilon$, $d_y = n_y \cdot \varepsilon$, where n_x, n_y are integers and ε is the pixel resolution of the interferometer. Following matrix relationship model can be established to recover the absolute reference surface form error. Denote the surface figure matrix of the test flat and the reference surface as $\mathbf{T}(i, j)$ and $\mathbf{R}(i, j)$, respectively, where i and j denote the pixel coordinates corresponding to CCD of interferometer. $i = 1 : N$ and $j = 1 : N$, where N means that there are N rows and columns in matrix representing the tested error map. Ignoring the measurement noise and considering the misalignments aberration when test a flat, the three measurement matrixes can be denoted as

$$\mathbf{M}_0(i,j) = \mathbf{R}(i,j) + \mathbf{T}(i,j) + \mathbf{t}_0 [i,j,1]^{\mathrm{T}}, \quad (1)$$

$$\mathbf{M}_x(i,j) = \mathbf{R}(i+n_x,j) + \mathbf{T}(i,j) + \mathbf{t}_x [i,j,1]^{\mathrm{T}}, \quad (2)$$

$$\mathbf{M}_y(i,j) = \mathbf{R}(i,j) + \mathbf{T}(i,j+n_y) + \mathbf{t}_y [i,j,1]^{\mathrm{T}}, \quad (3)$$

where $\mathbf{t}_m = [a_m, b_m, c_m]$ is the measurement index and $m = 0, x, y$) are the yaw, roll, and piston coefficients due to the misalignment of the test flat relative to the reference surface. Transform Eq. (1) and subtract it from Eq. (2) to get the difference matrix of surface form at two positions as

$$\mathbf{M}_y(i+n_x,j) - \mathbf{M}_x(i,j) = \mathbf{R}(i+n_x,j) - \mathbf{R}(i,j) + \mathbf{t}_0 [i+n_x,j,1]^{\mathrm{T}} - \mathbf{t}_x [i,j,1]^{\mathrm{T}}, \quad (4)$$

Flatten the matrix of difference surface (left side of Eq. 4) by rows into a column vector $\mathbf{d}_{0x}$. Then flatten the matrix $\mathbf{R}(i, j)$ by rows into a column vector $\mathbf{r}$. Set $\mathbf{t}_0 = 0$ and denote vector $\mathbf{g}$ as $[\mathbf{t}_x \ \mathbf{t}_y]^{\mathrm{T}}$. Then we have

$$\mathbf{d}_{0x} = \begin{bmatrix} \mathbf{G}_{0x} & \mathbf{D}_{0x} \end{bmatrix} \begin{bmatrix} \mathbf{g} \\ \mathbf{r} \end{bmatrix}, \quad (5)$$

where $[\mathbf{G}_{0x} \ \mathbf{D}_{0x}]$ is the relation matrix and can be deduced from Eq. 4.

Similarly, the translation at y direction can be obtained by combining Eq. (3) with Eq. (1). Further, a simultaneous equation can be obtained as

$$\begin{bmatrix} \mathbf{d}_{0x} \\ \mathbf{d}_{0y} \end{bmatrix} = \begin{bmatrix} \mathbf{G}_{0x} & \mathbf{D}_{0x} \\ \mathbf{G}_{0y} & \mathbf{D}_{0y} \end{bmatrix} \begin{bmatrix} \mathbf{g} \\ \mathbf{r} \end{bmatrix}. \quad (6)$$

Eq. 6 is a set of linear equations that can reconstruct the reference surface, i.e., $\mathbf{r}$ in the equation without theoretical error except the 2 order terms (i.e., x^2, y^2, and xy). However, for the solution to exist, the pixel of translation must be equal to 1, which means $n_x = n_y = 1$.

The single shear-shift requires that the translation is equal to the resolution of the calibration, hence the higher resolution leads to smaller translation which means lower signal-to-noise ratio. Xue [12] proposed that the linear equation set of the single shear-shift with a large translation not equal to 1 can also be solved using the least squares method. However, the result exhibit periodic error, which hardly meet the calibration with extreme precision required. In order to achieve large translation and high lateral resolution at the same time, the two shear-shift method is proposed [15]. The principle of the two shear-shift can be extended from the above mathematical. Figure 1(b) displays the two shear-shift test requires 5 shear-apertures with positions where $d_m = n_m \cdot \varepsilon$, $m = 0, x_1, x_2, y_1, y_2$. A quartic difference of five positions can produce an equation set similar as Eq. (6) which can also reconstruct the reference surface with no theoretical error except for the 2 order terms on the condition that these five shear-apertures positions meet the requirements of Eq. (7) as follows

$$\begin{cases} \mathrm{GCD}(n_{x1}, n_{x2}) = 1 \\ \mathrm{GCD}(n_{y1}, n_{y2}) = 1 \\ N \geq n_{x1} + n_{x2} \\ N \geq n_{y1} + n_{y2} \\ n_{x1}, n_{x2}, n_{y1}, n_{y2} \geq 1 \end{cases}, \quad (7)$$

where $\mathrm{GCD}(n_{x1}, n_{x2}) = 1$ means that the greatest common divisor of n_{x1} and n_{x2} is 1.

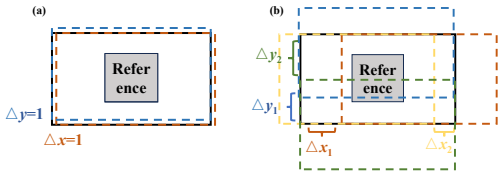

Figure 1. Schematic diagram of shear-shift. (a) Single shear-shift by 1 pixel. (b) Two shear-shift with five positions.

3. Simulations of test parameters and test error source

The shear ratio, defined as the ratio of shear displacement to the reference surface dimension along the translation axis, constitutes the principal operational parameter in the TSS absolute test methodology. To comply with the constraints imposed by Equation (7), this ratio must be maintained below 0.5. This parameter governs the overlapping proportion between differentiated surface regions—lower ratios increase overlapping regions, thereby satisfying Equation (7) requirements and mitigating random form errors in test flats, albeit with heightened susceptibility to measurement noise. Notably, shear-induced motion errors exhibit displacement-dependent characteristics. In our experimental configuration employing an 8.6 mm reference surface, practical displacement ranges remain constrained below 4.3 mm. As demonstrated in prior investigations [16], motion inaccuracies and alignment errors under such conditions contribute negligibly to measurement uncertainty. Consequently, our analysis prioritizes environmental disturbances as the dominant error source. Through systematic development of a physics-based model encompassing both the measurement system and environmental perturbation mechanisms, we executed parametric simulations to quantify shear ratio effects on calibration accuracy. This computational framework enabled identification of optimal operational parameters satisfying the stringent accuracy thresholds (PV < 1 nm, RMS < 0.2 nm), ultimately yielding a generalized protocol for implementing absolute tests in practical WLI applications.

The experimental implementation of the TSS method was realized through a custom-designed test system, schematically illustrated in Figure 2. This configuration comprises three core subsystems: (1) a dual-axis shear translation assembly with an 8.6 mm reference surface, employing a PI V-817.176211E0 high-load linear stage (407 mm travel range) for x-axis displacements and a PI UPL-120 precision stage (6635921130-0001, 13 mm travel range) for y-axis motions; (2) a focusing adjustment module utilizing an M511.DD high-resolution z-axis stage; and (3) a two-axis tilt compensation system integrating a PRS-200 rotary stage (6449921111) and WT-90 pitch stage (65509201) for real-time fringe nulling adjustments during measurement sequences. To ensure operational precision, the entire system is mounted on an air-floating vibration isolation platform housed within a

thermal stabilization chamber maintaining temperature variations within ±0.04°C and relative humidity fluctuations below ±0.3% over 24-hour periods. This environmental control regime ensures sub-nanometer measurement stability critical for X-ray mirror characterization. Shear transformations are executed through coordinated displacements along orthogonal axes, while the z-axis module dynamically optimizes focal plane alignment. Notably, the maximum shear displacement remains constrained to 4.3 mm (50% of the reference surface dimension), a parameter boundary derived from Equation (7) constraints and prior motion error analyses.

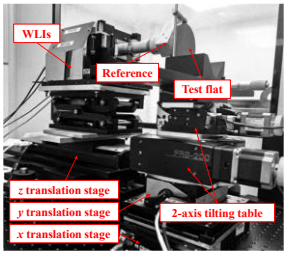

Figure 2. Sketch of the practical test system.

The error quantification protocol employed differential analysis between consecutive measurements to characterize short-term repeatability (minutes-scale temporal resolution) and comparative assessment of 24-hour separated measurements to evaluate long-term stability, with each dataset derived from 64-frame averaging to enhance measurement fidelity. Experimental results delineated in Figure 3 demonstrate the system's environmental sensitivity, exhibiting short-term repeatability errors of 0.268 nm PV / 0.047 nm RMS and 24-hour stability errors of 0.260 nm PV / 0.079 nm RMS. To isolate environmental disturbance effects from instrumental artifacts, Gaussian spline filtration (300 μm^{-1} low-pass cutoff) was systematically applied, suppressing high-frequency noise components (>1/300 μm spatial frequency) while preserving mid-spatial frequency features critical for X-ray mirror metrology.

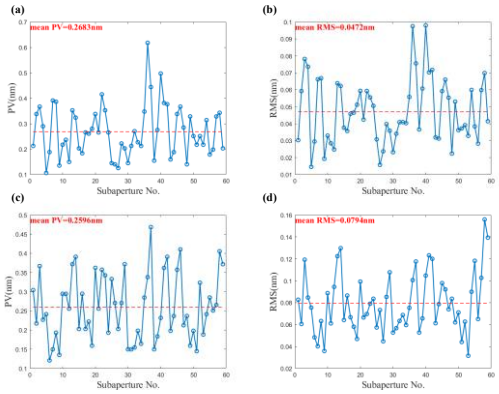

Figure 3. Environment disturbance. Short-term repeatability error (a) PV and (b) RMS. Long-term repeatability error (c) PV and (d)RMS.

Numerical simulations were conducted on a high-performance computing platform equipped with dual AMD EPYC 64-core processors and an NVIDIA RTX 4090 GPU, employing MATLAB 2024 for computational implementation. The simulation framework integrated two distinct surface profiles to emulate practical measurement conditions: a test surface derived from a silicon carbide calibration flat exhibiting a peak-to-valley (PV) form accuracy of 5.04 nm and root-mean-square (RMS) precision of 0.51 nm, alongside a reference surface reconstructed through iterative application of the random flats method. The reference surface generation involved fifty averaged measurements of an ultra-precision flat (PV 0.647 nm, RMS 0.127 nm) captured via the experimental system's 1× objective lens. As illustrated in Figure 4, the test surface intentionally exceeds the target calibration thresholds of PV 1 nm and RMS 0.2 nm, thereby establishing a conservative validation scenario, while the reference surface demonstrates enhanced precision through statistical averaging. This dual-profile configuration serves dual validation purposes—providing input parameters for the simulation model while enabling accuracy verification of the MSS calibration methodology detailed in Section 4. Although minor discrepancies exist between simulated and physical surface topographies, the selected profiles maintain sufficient metrological relevance for evaluating environmental disturbance effects. Consistent with experimental protocols, all surface data underwent Gaussian spline filtration with a 300 μm^{-1} low-pass cutoff to ensure spectral comparability between simulation and empirical results.

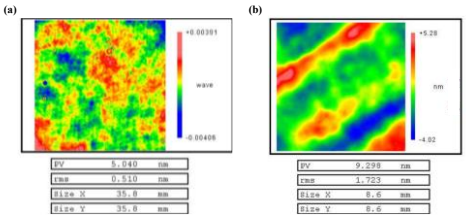

Figure 4. Input surfaces of simulation. Test flat (a) and reference (b).

Following model validation, simulation analyses were conducted to evaluate environmental disturbance impacts on calibration accuracy across different shear ratios. Five discrete shear ratios [0.02, 0.05, 0.1, 0.2, 0.4] were selected according to mathematical constraints derived from Equation (7). The experimentally measured environmental errors—including both short-term (consecutive measurement) and long-term (24-hour interval) repeatability data—were systematically incorporated into the simulation framework. As presented in Figure 5, the resulting profiles demonstrate the relationship between shear ratio selection and calibration error magnitude under these two disturbance regimes.

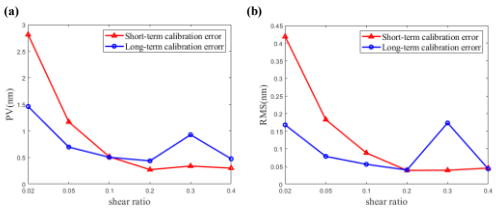

Figure 5. Calibration error with environment disturbance. Calibration error PV (a) and RMS (b).

The simulation results reveal distinct trends in reference calibration errors under varying shear ratios. For short-term environmental disturbances, both PV and RMS errors exhibit progressive reduction with increasing shear ratios, stabilizing at shear ratio=0.2 before demonstrating marginal elevation at higher values. Long-term disturbance patterns mirror this behavior, showing comparable error magnitudes across the tested shear ratio range. Optimal calibration performance was achieved at s=0.2, yielding short-term errors of 0.270 nm PV and 0.039 nm RMS and long-term errors of 0.434 nm PV and 0.040 nm RMS. This optimal shear ratio achieves minimum calibration errors while maintaining measurement stability under environmental disturbances.

4. Results

Experimental validation was performed using the test system illustrated in Figure 2, incorporating a Zygo NewView 9000 WLIs. Detailed specifications and alignment procedures for the translation stages are provided in Section 3. The test specimen consisted of a silicon carbide (SiC) calibration mirror with a surface accuracy of PV 5.04 nm and RMS 0.51 nm—intentionally exceeding the required calibration thresholds. A 1× Michelson objective lens (Model 6300-0524-02) served as the reference surface source. Preliminary surface characterization of both components, presented in Figure 4, confirmed their metrological suitability.

Guided by simulation results, the shear ratio was fixed at 0.2 during TSS implementation. Figure 6(a) displays the absolute calibration result for the reference surface, Figure 6(b) demonstrates PV 0.763 nm and RMS 0.155 nm errors in differential measurements between two 24-hour interval tests. Comparative analysis against the random flats method—utilizing an ultra-precision flat (PV 0.647 nm and RMS 0.127 nm)—revealed a maximum deviation of PV 0.232 nm and RMS 0.026 nm in Figure 6(c), confirming compliance with the PV < 1 nm and RMS < 0.2 nm accuracy requirements.

To evaluate parameter sensitivity, a control experiment employing a non-optimal shear ratio (shear ratio=0.02) was conducted under identical hardware conditions. As shown in Figure 7, this configuration resulted in degraded 24-hour reproducibility of PV 6.479 nm and RMS 0.575 nm and reduced agreement with the random flats method of PV 4.133 nm and RMS 0.665 nm, conclusively demonstrating the criticality of proper shear ratio selection for maintaining calibration accuracy.

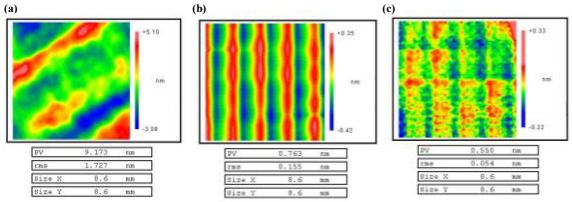

Figure 6. Experimental results. (a) Reference calibration result by TSS. (b) Reproductivity of TSS for 24 hours. (c) Accuracy through comparison with the random flats method.

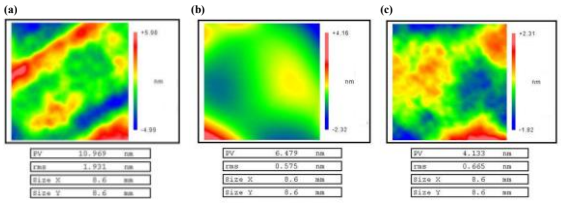

Figure 7. Results of comparison Experiment. (a) Reference calibration result with inappropriate shear ratio. (b) 24 hours reproductivity with inappropriate shear ratio. (c) Accuracy by comparing with the random flats method.

5. Discussion

1. The simulation and experimental findings collectively validate the efficacy of the TSS method in reconstructing reference surfaces without requiring prior knowledge of the test specimen's form accuracy. This approach provides a distinct advantage over conventional random flats methodology by eliminating both the necessity for surface form prediction and the dependency on ultra-precision reference flats.
2. Notably, the high spatial resolution of white-light interferometers introduces measurement artifacts comprising high-frequency form errors coupled with nonlinear systematic errors. Effective data processing therefore becomes imperative for achieving target accuracy thresholds. In accordance with manufacturing requirements, all experimental data underwent Gaussian spline filtration (300 μm^{-1} low-pass cutoff) to suppress non-deterministic high-frequency components irrelevant to surface shaping processes. Furthermore, second-order polynomial terms (x^2, xy, y^2), inherently unresolvable through translational shear operations without rotational components, were systematically excluded from the analytical framework.
3. Experimental observations additionally reveal periodic error signatures inherent to the TSS algorithm's mathematical formulation. Subsequent research directions should focus on developing enhanced shear-shift techniques to mitigate these systematic errors and further improve calibration precision.

6. Conclusion

This study introduces a TSS absolute calibration method for WLIs reference surface, combining theoretical model with experimental validation. A comprehensive framework was established through three interconnected components: mathematical model of shear-shift operations, development of a physics-based virtual calibration platform incorporating experimental error profiles, and implementation of an environmentally controlled multi-axis testbed. Systematic environmental disturbance analysis identified an optimal shear ratio of 0.2, balancing measurement sensitivity and error suppression. Experimental validation using a SiC calibration of PV 5.04 nm and RMS 0.51 nm demonstrated sub-nanometric calibration accuracy of PV 0.550 nm and RMS 0.054 nm through rigorous comparison with the random flats method. Notably, the TSS technique eliminates the requirement for ultra-precision reference flats mandated by conventional approaches while achieving compliance with stringent calibration accuracy of PV < 1 nm and RMS < 0.2 nm. This advancement significantly enhances WLIs metrological capabilities for next-generation synchrotron optics fabrication, particularly in scenarios involving strongly curved surfaces or limited access to reference standards.

References

[1] Thiess H, Lasser H and Siewert F 2010 *Nucl. Instrum. Methods Phys. Res. Sect.A* **616** 2-3 157-61
[2] Yamauchi K, Mimura H and Inagaki K et al 2002 *Rev. Sci. Instrum.* **73** 4028-33
[3] Groot P 2021 *J. Phys. Photonics* **3** 24004
[4] Damian V, Bojan M, Schiopu P, Iordache I, Ionita B and Apostol D 2009 *Proc. SPIE* **7297** 1H
[5] Yamauchi K, et al 2003 *Rev. Sci. Instrum.* **74** 2894-98
[6] Assoufid L, et al 2007 *Proc. SPIE* **6704** 06
[7] Rommeveaux, Amparo Vivo Esrf. Fr, Barrett and Raymond 2010 *Nucl. Instrum. Methods Phys. Res. Sect. A* **616** 2-3 183-87
[8] Creath K, and Wyant J 1990 *Appl. Opt.* **29** 3823-27
[9] Keenan P 1983 *Proc. SPIE* **429** 042901
[10] Quan HY, Hou X, Wu F and Song WH 2015 *Opt. Express* **23** 1630-19
[11] Huang Y, Ma J, Zhu RH, Yuan CJ, Chen L, Cai HJ and Sun WY 2015 *Opt. Express* **23** 29687-97
[12] Xue S, Chen S, Zhai D and Shi F 2017 *Opt. Commun.* **389** 133-43
[13] Leibbrandt G, Harbers G and Kunst P 1996 *Appl. Opt.* **35** 6151-61
[14] Brug H 1997 *Appl. Opt.* **36** 2788-90
[15] Zhai D, Chen S, Xue S and Yin ZQ 2016 *Appl. Opt.* **55** 8063-69
[16] Liu Y, Jian H, Xue S, Gao X, Hu Z, Huang A and Dai,Y 2024 *Opt. Express* **32** 35623-41